Quantum dot microcavity control of photon statistics

Snijders, H.J.

Chapter 4

Purification of a single photon non-linearity

We show that the lifetime-reduced fidelity of a semiconductor QD–cavity single photon nonlinearity can be restored by polarization pre- and postselection. This is realized with a nearly polarization degenerate microcavity in the weak coupling regime, where an output polarizer enables quantum interference of the two orthogonally polarized transmission amplitudes. This allows us to transform incident coherent light into a stream of strongly correlated photons with a second-order correlation function of $g^{(2)}(0) \gtrsim 40$, larger than previous experimental results even in the strong-coupling regime. This purification technique might also be useful to improve the fidelity of QD based logic gates.

This Chapter has been published in Nature Communications 7, 12578–12578 (2016) [5].

4.1 Introduction

photon nonlinearities enabled by quantum two-level systems are essential for future quantum information technologies, as they are the building block of quantum photonics logic gates [21], deterministic entanglers of independent photons [54], and for coupling distant nodes to form a quantum network [22]. Near unity fidelity interaction of photons with a two-level system such as an atom or QD is enabled by embedding it into an optical cavity [55]. Then, the electronic and photonic states become bound and form the dressed states [15] of cavity quantum electrodynamics (CQED). A hallmark of single-photon nonlinearities is the modification of the photon statistics of a quasi-resonant weak coherent input beam [56]: The transmitted photon statistics can become antibunched due to the photon-blockade effect [21, 57, 58], which is enabled by the anharmonicity of the Jaynes–Cummings ladder [59, 60, 61]. The system can also be tuned to reach the regime of photon tunnelling [62, 56] where the single-photon component is reduced and photons are transmitted in $N > 1$ Fock states or "photon bundles" [63, 64]. This regime is called photon tunneling since it is the opposite of the photon-blockade effect.

In terms of the second-order photon correlation function $g^{(2)}(0)$, values up to ~ 2 [65, 66, 67, 68] have been obtained experimentally with QDs, which hardly exceeds even the classical case of thermal light following Bose statistics of $g^{(2)}(0) = 2$. In atomic systems with much longer coherence times, values up to ~ 50 have been obtained [56], and it is known [69] that strict two-photon light sources exhibit diverging $g^{(2)}(0)$ if the two-photon flux is reduced. Most related QD experiments to date have been operating in the strong-coupling regime of CQED, which is considered to be essential due to its photon-number dependent energy structure [66, 56, 68]. In the weak-coupling regime, the coupling of cavity and QD is reduced, leading to reduced QD contrast as shown in Fig. 4.1b (black curves). The strong coupling regime, however, requires a small optical mode volume, which in turn makes it extremely hard to achieve polarization degeneracy of the fundamental cavity mode. This is due to unavoidable deviations from the ideal shape and intrinsic birefringence [70, 71] on the GaAs platform, precluding implementation of deterministic polarization-based quantum gates [54, 72, 47]. Here we show, using a nearly polarization degenerate cavity in the weak coupling CQED regime, that we can transform incident coherent light into a stream of strongly correlated photons with $g^{(2)}(0) = 25.7 \pm 0.9$, corresponding to $\gtrsim 40$ in the absence of detector jitter. The polarization degenerate cavity enables us to choose the incident polarization $\theta_{in} = 45°$ such that both fine-structure split QD transitions along $\theta^X_{QD} = 0°$ and $\theta^Y_{QD} = 90°$ are excited, and we can use a postselection polarizer behind the cavity (θ_{out}) to induce quantum interference of the two transmitted orthogonal polarization components (Fig. 4.1a). This leads to the appearance of two special postselection polarizer angles $\theta^{*\pm}_{out}$ (depending on sample parameters), which can be used to restore perfect QD contrast (red curves in Fig. 4.1b). This compensates fully for reduced QD-cavity coupling due to finite QD lifetime and QD-cavity coupling strength, leading to complete suppression of transmission of the single-photon component in the low excitation limit. The transmission of higher-photon number states remains largely intact, allowing us to observe in Fig. 1c the strongest photon correlations to date in a solid-state system, reaching the range of strongly coupled atomic systems [56]. In the following a detailed experimental and theoretical investigation of this effect, which can be seen as a purification of a single-photon nonlinearity, will be presented.

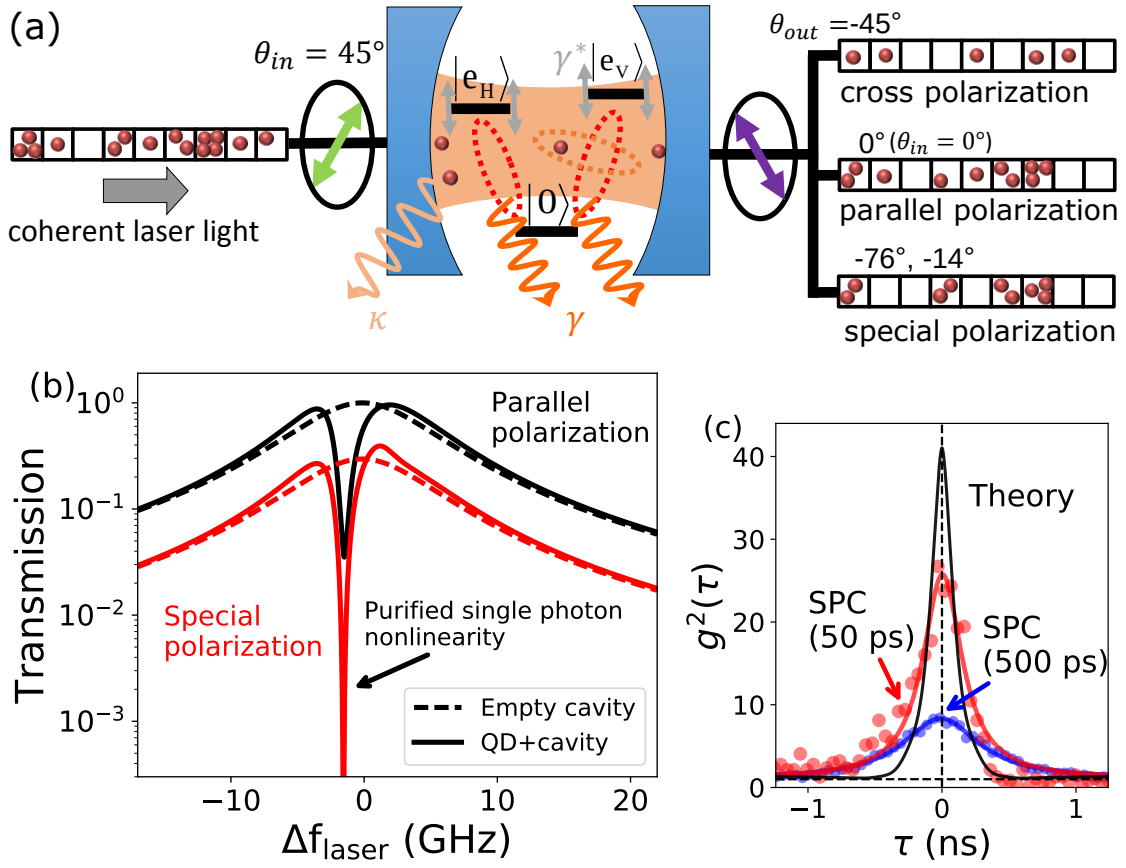

Figure 4.1: (a) Cartoon of the experiment: Polarization pre- and postselection in a resonant transmission CQED experiment enables tuning of the photon statistics from antibunched to bunched. (b) Theoretical resonant transmission spectra for coherent light with mean photon number $\ll 1$, with and without the QD, comparing the conventional case (parallel polarizers) to the case of special polarization postselection along θ^*_{out}: close to one of the QD resonances, single-photon transmission is perfectly suppressed, despite the finite lifetime and cavity coupling of the QD transition. (c) Second-order correlation function for the special polarization angle case, comparing theory and experiment using two different sets of single-photon counters (SPCs) with different timing jitter, 50 ps and 500 ps.

4.2 Device structure

Our device for the experiment performed in this chapter consists of self-assembled InAs/GaAs QDs embedded in a micropillar Fabry-Perot cavity grown by molecular beam epitaxy [73]. Two distributed Bragg reflectors (DBR) surround a $\sim 5\lambda$ thick cavity containing in the center InGaAs self-assembled QDs and an oxide aperture for transverse confinement. The top DBR mirror consists of 26 pairs of $\lambda/4$ thick GaAs / $Al_{0.90}Ga_{0.10}As$ layers, while the bottom mirror has 13 pairs of GaAs / AlAs layers and 16 pairs of GaAs / $Al_{0.90}Ga_{0.10}As$ layers. The QD layer is embedded in a P-I-N junction, separated by a 35 nm thick tunnel barrier from the n-doped GaAs:Si (2.0×10^{18} cm^{-3}) electron reservoir, to enable tuning of the QD resonance frequency by the quantum confined Stark effect. For transverse mode confinement and to achieve polarization degenerate cavity modes, we first ion-etch micropillars of large diameter (35 µm) and slightly elliptical shape, then we use wet-chemical oxidation of an 10 nm thick AlAs layer [74], which is embedded between 95 nm $Al_{0.83}Ga_{0.17}As$ and 66 nm thick $Al_{0.75}Ga_{0.25}As$, to prepare an intracavity lens for transverse-mode confinement [75], avoiding loss by surface scattering at the side walls. Finally, we fine-tune the cavity modes by laser induced surface defects [27, 26] to obtain a polarization mode splitting much smaller than the cavity linewidth.

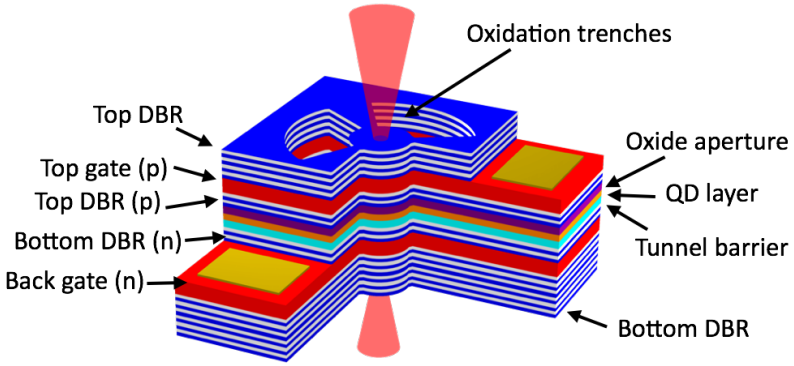

Figure 4.2: Scheme of the device.

4.3 Theoretical model

The system we study here is tuned to contain a single neutral QD within the cavity linewidth. The excitonic fine-structure splitting leads to 4.8 GHz splitting between the orthogonally polarized QD transitions at 0° (ω_{QD}^{Y}) and 90° (ω_{QD}^{X}). The fundamental cavity modes show a residual polarization splitting of 4 GHz ($f_c^X = 0$ GHz, $f_c^Y = -4$ GHz), and the cavity axes are rotated by 5° with respect to the QD axes. We describe the QD-cavity system via an extended version of a two-level system in an optical cavity, which is driven by a classical coherent laser field. Albeit our cavities have only a small polarization splitting of the fundamental modes, we take full care of it. The quantum description, based on the application of a unitary transformation to transform the Hamiltonian from a time-dependent to a time-independent form and the rotating-wave approximation, results in the following Hamiltonian ($\hbar = 1$)[15, 72]:

$$
\begin{aligned}
H \;=\; & \left(\omega_L-\omega_c^X\right)\hat{a}_X^\dagger\hat{a}_X+\left(\omega_L-\omega_c^Y\right)\hat{a}_Y^\dagger\hat{a}_Y+\left(\omega_L-\omega_{QD}^X\right)\hat{\sigma}_X^\dagger\hat{\sigma}_X \\
& +\left(\omega_L-\omega_{QD}^Y\right)\hat{\sigma}_Y^\dagger\hat{\sigma}_Y+g_Y\left(\hat{\sigma}_Y\hat{b}_Y^\dagger+\hat{\sigma}_Y^\dagger\hat{b}_Y\right)+g_X\left(\hat{\sigma}_X\hat{b}_X^\dagger+\hat{\sigma}_X^\dagger\hat{b}_X\right) \\
& +\tfrac{\eta}{2}\left[e_x'\left(\hat{a}_X^\dagger+\hat{a}_X\right)+e_y'\left(\hat{a}_Y^\dagger+\hat{a}_Y\right)\right]+\tfrac{1}{2}(\omega_c^X-\omega_c^Y)\left[\hat{a}_X^\dagger\hat{a}_Y+\hat{a}_Y^\dagger\hat{a}_X\right]
\end{aligned}
\tag{4.1}
$$

Here $\omega_c^{X/Y}$ are the cavity resonance frequencies of the polarized cavity modes, and $\omega_{QD}^{X/Y}$ are the fine-structure-split QD transition frequencies. $\hat{a}_{X/Y}^\dagger$ is the photon creation operator for a photon in X/Y polarization, and $\hat{\sigma}_{X/Y}^\dagger$ creates an X/Y polarized neutral exciton. The terms with coupling constants $g_{X/Y}$ describe the interaction between a QD transition and the cavity field, which is rotated into the QD polarization basis by $\hat{b}_X=\hat{a}_X cos\,\phi+\hat{a}_Y sin\,\phi$ and $\hat{b}_Y=-\hat{a}_X sin\,\phi+\hat{a}_Y cos\,\phi$, where ϕ is the rotation angle. This Hamiltonian is designed for a cavity with a small polarization splitting. The last term describes the driving of the cavity by an external linearly polarized coherent laser field, where η^2 is proportional to the incident intensity [16], and the Jones vector $\left(e_x', e_y'\right)$ describes the incident light polarization.

Next we write down a quantum master equation for our Hamiltonian and include Lindblad-type dissipation for the cavity decay rate κ, the population relaxation rate $\gamma_{||}$ and the total pure dephasing rate γ^*.

$$
\frac{d\rho}{dt}=\mathfrak{L}\rho=-i\left[\hat{H},\rho\right]+\sum_{j=X,Y}\kappa\mathfrak{D}[\hat{a}_j]\rho+\gamma_{||}\mathfrak{D}[\hat{\sigma}_j]\rho+\frac{\gamma^*}{2}\mathfrak{D}[\hat{\sigma}_{zj}]\rho, \tag{4.2}
$$

Where ρ is the density matrix of the QD-cavity system, $\mathfrak{L}$ is the Liouvillian superoperator for QD-cavity density matrix and $\mathfrak{D}[\hat{o}]\rho\equiv\frac{1}{2}\left[2\hat{o}\rho\hat{o}^\dagger-\hat{o}^\dagger\hat{o}\rho-\rho\hat{o}^\dagger\hat{o}\right]$ results in Lindblad-type dissipation. Here $\hat{\sigma}_{zj}$ is defined as $\frac{1}{2}\left(\hat{\sigma}_j^\dagger\hat{\sigma}_j-\hat{\sigma}_j\hat{\sigma}_j^\dagger\right)$. The validity of Eq. 4.2 is similar to the arguments given in section 3.1.

4.3.1 Transmission and photon correlations

The cavity transmittivity is calculated by $T=\mathrm{Tr}\left[\rho_0\left(e_1\hat{a}_X^\dagger+e_2\hat{a}_Y^\dagger\right)\left(e_1\hat{a}_X+e_2\hat{a}_Y\right)\right]=\mathrm{Tr}\left(\rho_0\hat{a}^\dagger\hat{a}\right)$, where (e_1,e_2) describes the output-polarizer Jones vector, and ρ_0 is the steady-state density matrix of the system. We investigate the photon correlations by calculating the second-order correlation function, which is independent of mirror loss and can therefore be calculated directly from the intracavity photon operators $\langle\hat{a}^\dagger\hat{a}\rangle$. The second-order correlation function is given by $g^{(2)}(\tau)=\frac{\langle\hat{a}^\dagger(0)\hat{a}^\dagger(\tau)\hat{a}(\tau)\hat{a}(0)\rangle}{\langle\hat{a}^\dagger(0)\hat{a}(0)\rangle^2}$ with the time-dependent photon creation operator $\hat{a}^\dagger(\tau)$. In order to solve the time-dependence of the operator $\hat{a}^\dagger(\tau)$, we assume that the effect of the operator $\mathfrak{L}$ is small and the eigenvalues are non-degenerate, which allows us to write $\hat{a}^\dagger(\tau)$ as $\hat{a}^\dagger e^{\mathfrak{L}\tau}$. The effect of the operator $\mathfrak{L}$ is small if it acts on a steady-state density matrix [76].

4.3.2 Estimation of model parameters

For estimation of the parameters, we fit the theory above discussed to the experimental transmission data for 6 different output polarizations for $\theta_{in}=45°$, i.e., both QD transitions are excited. The result in Fig. 4.3 shows decent agreement between experiment

(black curve) and theory (red curve). We obtain the best-fit parameters $\kappa = 105 \pm 3$ ns^{-1}, $g = 14 \pm 0.1$ ns^{-1}, $\gamma^{||} = 1.0 \pm 0.4$ ns^{-1}, $\gamma^* = 0.6 \pm 0.01$ ns^{-1}, $f_{QD}^{X/Y} = -2.4/2.4$ GHz. The residual cavity polarization splitting is 4 GHz ($f_c^X = 0$ GHz, $f_c^Y = -4$ GHz), where the $\{X, Y\}$ axes are rotated by $\phi = 5°$ with respect to the QD axes. We note that another QD is visible within the cavity resonance, compare Fig. 4.3 for $\theta_{out} = 90°$ at around -10 GHz; but since it is much less strongly coupled to the cavity mode it can be neglected.

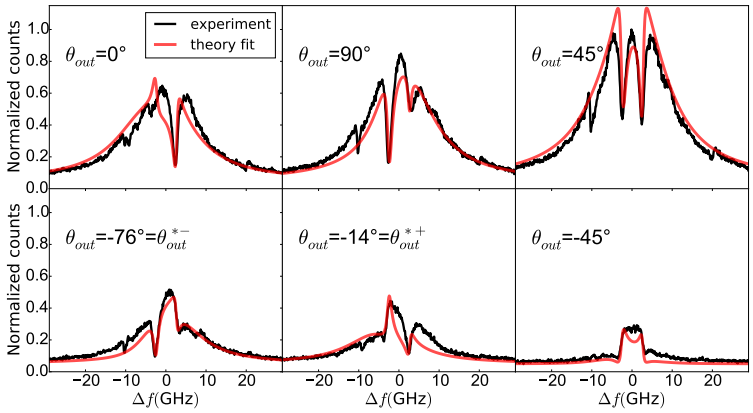

Figure 4.3: Experimental data (black) and the theoretical fit (red) . The input polarization was set to $\theta_{in} = 45°$ and θ_{out}^{*+} and θ_{out}^{*-} indicate the special polarization angles.

4.4 Resonant photon correlation spectroscopy

We use a narrow band (100 kHz) laser to probe the system and study the transmitted light (Fig. 4.1a), as a function of laser frequency and postselection polarizer angle behind the cavity. For each set of parameters, we measure the resonantly transmitted light intensity and its second-order photon correlation function $g^{(2)}(\tau)$ using a Hanbury Brown Twiss setup. The discrete nature of the QD levels leads to a strongly nonlinear response of the system depending on the incident photon-number distribution; we operate at low intensities to avoid saturation effects. We show here only data for an incident polarization $\theta_{in} = 45°$. Under this angle both QD transitions are equally excited.
First, we compare experimental and theoretical resonant transmission measurements in Fig. 4.4, where the coherent-light transmittivity as a function of the laser detuning and orientation of the output polarizer angle θ_{out} is shown. For clarity, we have normalized the traces for each polarization setting. The horizontal lines indicate the QD fine-structure split transitions (ω_{QD}^X, ω_{QD}^Y), the black circles indicate regions of low transmission and the vertical dashed lines the special polarization angles $\theta_{out}^{*+} \approx -14°$, $\theta_{out}^{*-} \approx -76°$. From comparison of both panels in Fig. 4.4, we find excellent agreement between experiment and theory.

Now we perform photon correlation measurements; instead of tuning the laser, we tune the QD, the reference are the cavity modes. Because the cavity linewidth is large compared to the QD tuning range in Fig. 4.5, there is nearly no difference compared

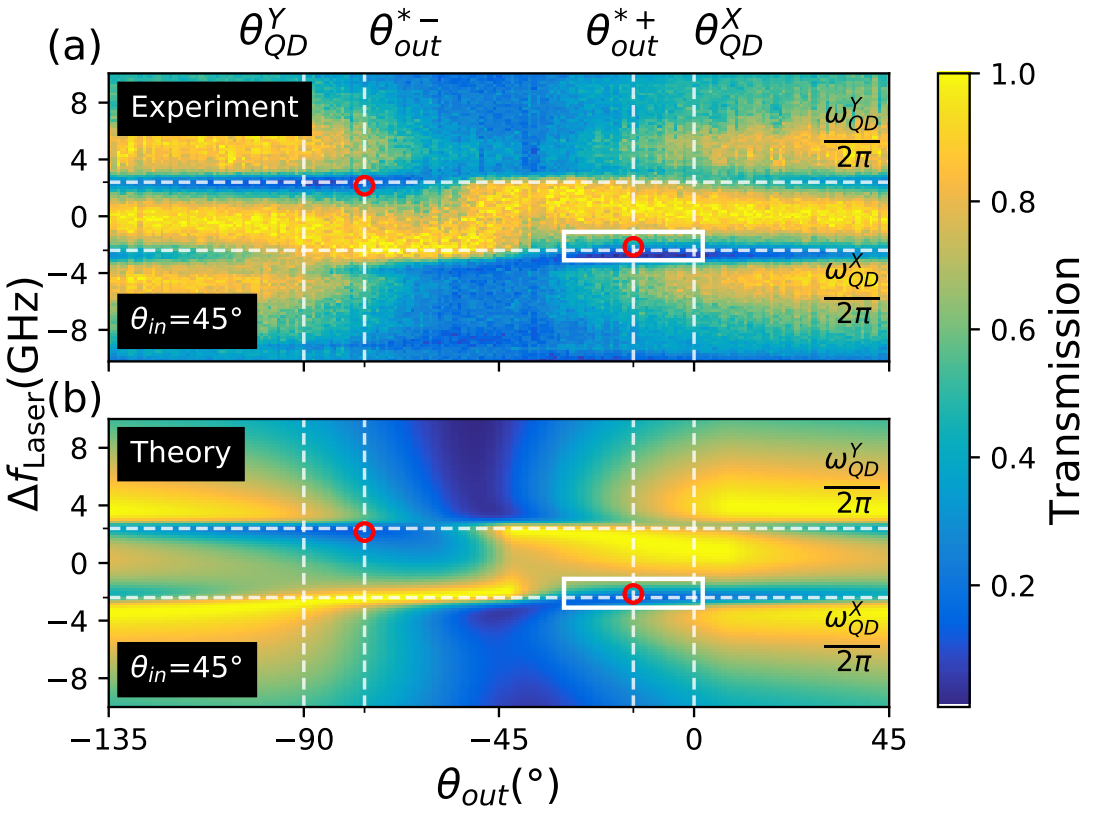

Figure 4.4: Experimental (a) and theoretical (b) false color plot of the column wise normalized optical transmission as a function of the laser detuning Δf_{Laser} and the polarization θ_{out} ($\theta_{in} = 45°$). The fine-split QD transition frequencies are at $f_{QD}^{X} = -2.4$ GHz and $f_{QD}^{Y} = 2.4$ GHz. The red circles indicate the special polarization conditions; the white square indicates the area explored in Fig. 4.5.

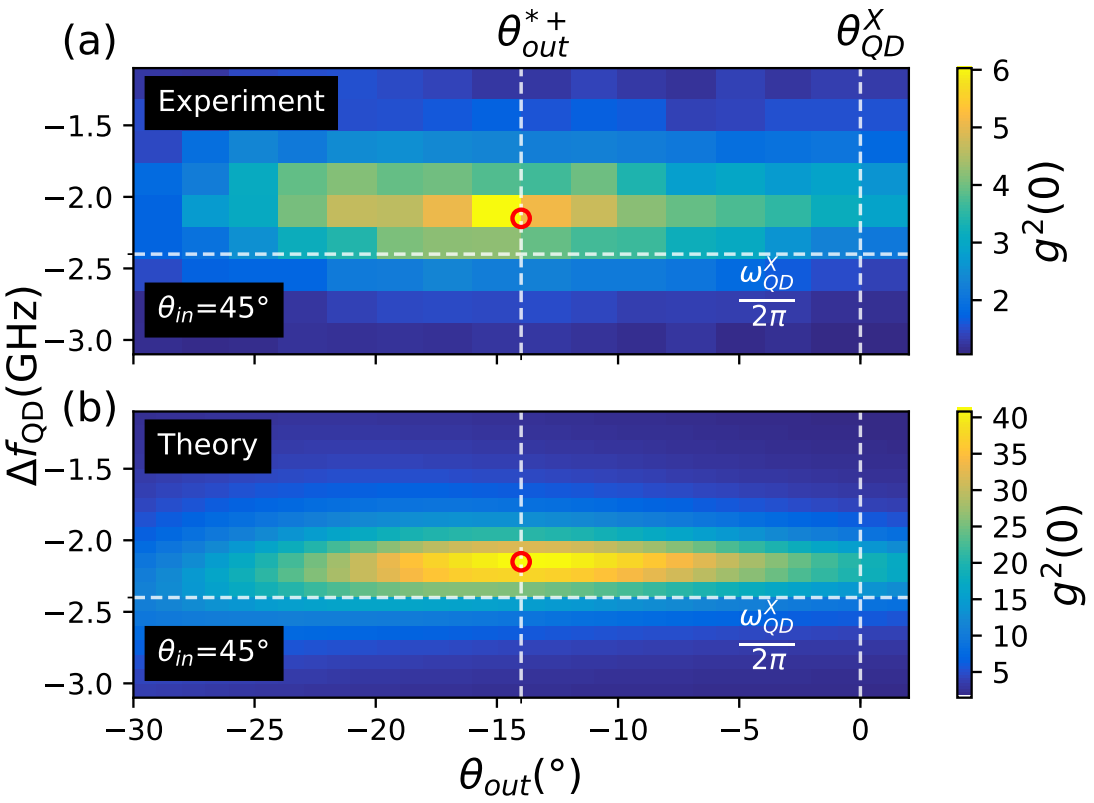

Figure 4.5: Experimental (a) and theoretical (b) data of the second-order correlation function as a function of the QD frequency and output polarization (θ_{out}), taken in the area marked with a white rectangle in Fig. 4.4. The vertical dashed lines indicate the special polarization angle and the QD axes, and the horizontal line the QD resonance frequency.

to tuning the laser. Experimentally, using an external electric field to tune the QD via the quantum-confined Stark effect is much more robust than laser-frequency tuning. Fig. 4.5 shows the false-color map of $g^{(2)}(0)$ as function of output polarization θ_{out} and QD detuning. We see clearly that the enhanced bunching occurs under the special polarization condition in the low-transmittivity regions indicated in Fig. 4.4. This is expected as in weak coherent light beams, the P_1 single-photon component is dominating, and removal thereof should lead to enhanced bunching. The theoretical simulation (Fig. 4.5b) shows a maximal photon bunching of $g^{(2)}(0) \approx 40$. Compared to this, the experimentally observed photon correlations are less ($g^{(2)}(0) \approx 6$), which is due to the detector response: Fig. 4.5a was recorded with a 500 ps timing-jitter detector, if we repeat the measurement at the special polarization angle with a 50 ps timing-jitter detector (the corresponding $g^{(2)}(\tau)$ measurements are compared in Fig. 4.1b), we obtain $g^{(2)}(0) = 25.7 \pm 0.9$. Both results agree very well to the convolution of the theoretically expected $g^{(2)}(\tau)$ with the detector responses (Fig. 4.1b); see also section 4.6.

4.5 Discussion

We have shown by experiment and theory that the reduced fidelity of a QD nonlinearity, caused by imperfect QD-cavity coupling, can be strongly enhanced by pre- and post-selection of specific polarization states. This enables transformation of a weak coherent input beam into highly bunched light with $g^{(2)}(0) \gtrsim 40$, a value that has not been reached before, not even in the strong coupling regime. How is it possible to reach such high photon correlations, how does the polarization-based purification technique work?

We consider incident light with a frequency in the vicinity of one of the QD resonances, say ω_{QD}^{X}, and let us decompose the electromagnetic field transmitted through the cavity in two orthogonally polarized components: the *signal* Field E_S polarized along the QD resonance polarization $\theta_{QD}^{X} = 0°$, and the *local oscillator* E_{LO} which has interacted with an empty cavity because it is polarized orthogonally to θ_{QD}^{X}. Now, we consider three cases: (i) efficient interaction of the QD with incident light (cooperativity $C > 1$), (ii) intermediate interaction ($C \approx 1$), and (iii) weak interaction ($C \to 0$). The special polarization angles for various cooperativities are shown in Fig. 4.6.

In case (i), the QD leads to a nearly complete removal of the single-photon component from the incident coherent light polarized along the QD polarization: these photons are in principle perfectly reflected from the cavity and we simply have to detect along the same axis ($\theta_{out}^{*} = \theta_{QD}^{X} = 0°$, see Fig. 4.6) to observe strong photon correlations. A significant proportion of higher photon-number states are transmitted. Since the second-order correlation function can be expressed in terms of the photon-number distribution as $g^{(2)}(0) \propto 2\,P_2/P_1^2$ (ignoring $N > 2$ photon-number states), which for $P_2 \ll P_1$ and $P_{N>2} \ll P_2$, this leads to diverging photon correlations like $g^{(2)}(0) \propto 1/\alpha^2$ if the single-photon component is attenuated as $P_1 \to \alpha P_1$.

Now in case (ii), for realistic systems, the finite lifetime of the QD transition and/or limited QD-cavity coupling g leads to a reduced cooperativity: Even in the low-excitation limit, not every single-photon state is filtered out. Therefore, the signal field E_S contains a fraction of coherent light reducing the photon bunching along the QD polarization θ_{QD}^{X}, compare Fig. 4.5. This effect has been called "self-homodyning" in literature [77, 78]. With the purification technique, we now rotate the postselection polarizer to interfere a portion of the local oscillator field E_{LO} with the signal field, leading to the *superimposed* field $E_{SL} = e^{i\phi_S} E_S + e^{i\phi_{LO}} E_{LO}$ [79]. The polarizer angle controls the relative intensity of the two components, and we can control the transmission phases ϕ_S and ϕ_{LO} by adjusting the laser frequency, because the phases vary strongly in the vicinity of the QD and cavity resonances. We simply have to choose the local oscillator intensity such that it matches the intensity of the portion of E_S, and adjust the phases for destructive interference. The result is that we detect in transmission mainly the single-photon filtered portion of E_S, which leads to very high photon correlations in the transmitted light despite limited cooperativity.

Finally, in case (iii) for $C \to 0$, only a vanishing fraction of the photons have interacted with the QD. We have to tune the postselection polarizer to $-45°$ to destructively interfere nearly equal amounts of E_S and E_{LO} to observe enhanced photon correlations. This case is similar to that recently investigated in [80], where (weak) photon bunching is observed for a relative phase of π ($\phi_S - \phi_{LO} = \pi$). We have a high-finesse ($F \approx 800$) cavity and significant cooperativity, which enables us to observe much stronger photon correlations.

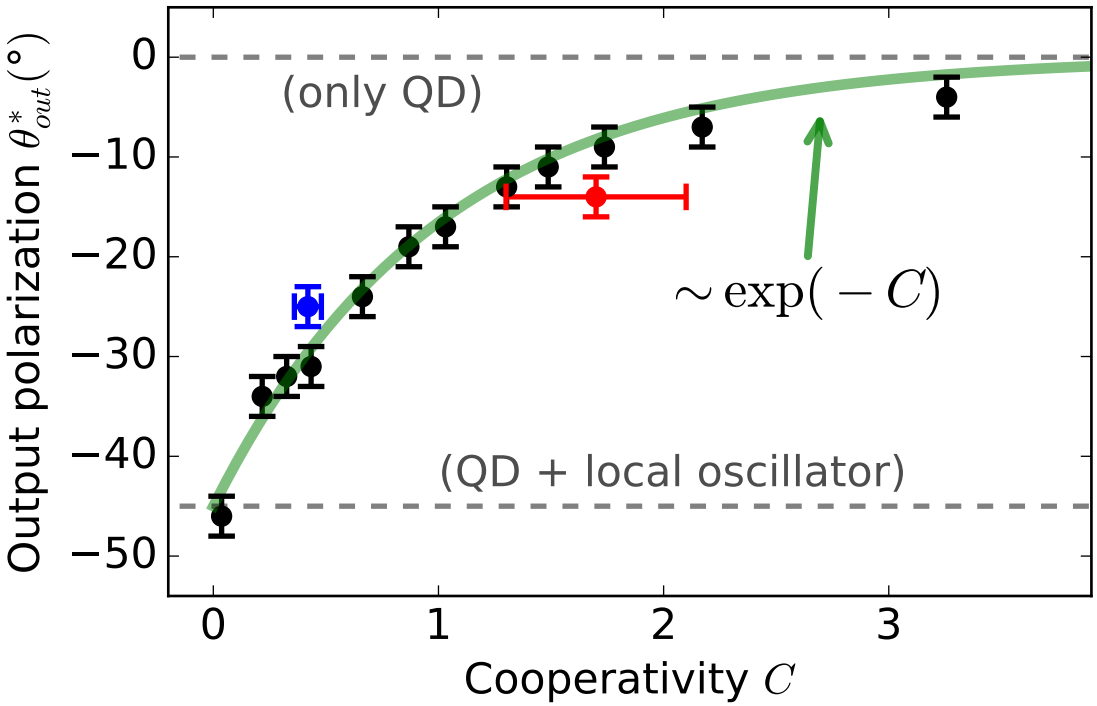

Figure 4.6: Numerically determined special polarization angle, where photon bunching in transmission is maximized, as a function of the cooperativity C, which in turn is modified by varying only the QD lifetime $\gamma_{\parallel}$. The green curve is given by the phenomenological expression $-45° \exp(-C)$: In the limit of high C, the QD alone can efficiently filter out single-photon states leading to photon bunching. But for low cooperativity C, it is advantageous to mix the quantum-dot scattered light with a "local oscillator" provided by orthogonal polarization. The error bars are due to numerical errors in optimization of the laser frequency.

The special postselection angle θ^*_{out} and laser frequency have to be optimized numerically in principle because pure dephasing cannot be taken care of in a semi-classical model. Despite this, we found that the special polarization angle shows approximately a very simple dependency on the cooperativity $\theta^*_{out} \approx -45° \exp(-C)$, see Fig. 4.6, which agrees well to our intuitive explanation here.

As a last point, we analyze the strong photon bunching in terms of the photon-number distribution P_n. We use our theoretical model to determine P_n, as direct experimental determination thereof is strongly complicated by its sensitivity to loss. But also the simulation of narrow-band photon-number Fock input states is challenging in the quantum master model [81]. Therefore we use coherent input light, and analyze the intracavity light in terms of its polarized photon-number distribution, taking care of quantum interference at the postselection polarizer acting on the intracavity field. This is an approximation because imperfect transmission through the cavity reshapes P_n. We found that the photon statistics P_n can be calculated best by projection on the required Fock states using

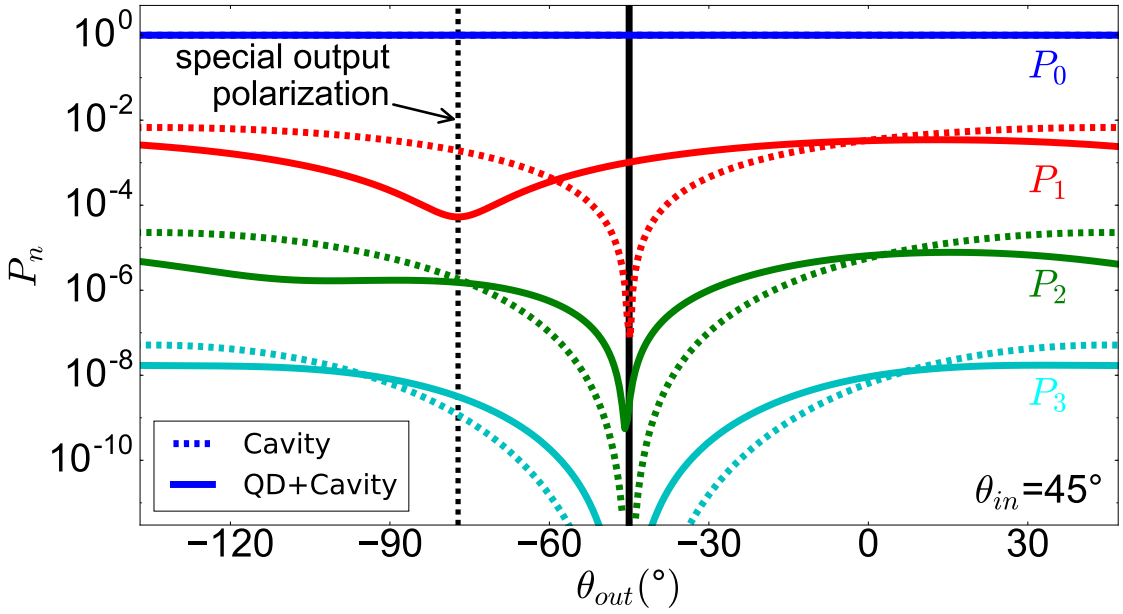

Figure 4.7: Calculated photon-number distribution after the polarizer, with (through curves) and without (dashed curves) coupling to the QD in the cavity, the laser frequency is set to one of the QD resonances. With QD, we clearly see the photon-number dependent shift of the transmission dip. Only the photon-number distribution of the detected polarization component is shown, therefore the total number of photons in case with QD can exceed the case without QD due to polarization conversion by the dot. For clarity, pure dephasing has been neglected here, making the special polarization angle different from the other simulations and experimental results.

polarization-rotated Fock-space ladder operators $b^\dagger_{x/y} = a^\dagger_{x/y}\cos\theta_{out} \mp a^\dagger_{y/x}\sin\theta_{out}$, and tracing out the undesired polarization component afterwards. With the numerically [38] calculated steady-state density matrix operator ρ of our system, we obtain the photon-number distribution after the polarizer:

$$P_n = \sum_{m=0}^{N} \frac{1}{n!\,m!} \langle 0_x 0_y | \, (b_x)^n \, (b_y)^m \, \rho \, \left(b_x^\dagger\right)^n \left(b_y^\dagger\right)^m | 0_x 0_y \rangle \tag{4.3}$$

Fig. 4.7 shows the 4 lowest photon-number probabilities as a function of the polarizer angle θ_{out}, for the case with and without QD. In the empty-cavity case we see, as expected, lowest transmission under the cross-polarization condition ($\theta_{out} = -45°$). For the case with the QD, we observe a photon-number dependent shift of the transmission dip. At the special polarization angle θ^*_{out}, we see that the one-photon component reaches a minimum while the higher-photon number states do not, which explains the enhanced photon bunching enabled by the purification technique.

It is important to note that also the two-photon transmission dip (P_2) is not exactly at cross-polarization, which suggests the following intuitive explanation: Apparently, in the photon-number basis, the different Fock states pick up a different phase during transmission through the QD-cavity system. In the weak coupling regime, but often also

in the strong coupling regime, the individual Jaynes–Cummings dressed states cannot be resolved spectrally because $g \lesssim \kappa$. However, the CQED system is still photon-number sensitive, which implies lifetime-dependent Jaynes–Cummings effects in the weak coupling regime: the decay rate of the CQED system increases with the number of photons in the cavity [82, 83]. As consequence, higher photon-number states have a modified interaction cross section and experience a reduced phase shift. The dip in P_2 in Fig. 4.7 is already very close to the cross-polarization angle $\theta_{out} = -45°$, while the dips for higher photon-number states $P_{n>2}$ are indistinguishable from $\theta_{out} = -45°$.

In conclusion, we found that the nonlinear response of a lossy cavity-QD system can be strongly enhanced by postselection of a particular polarization state. This leads to interference between Fock states that experience different modifications by the QD nonlinearity, and results in strong photon correlations of the transmitted light. As the underlying effect, interference of the two polarization modes leads to high-fidelity cancellation of the single-photon transmission for the special polarization postselection. By correlating the results with a theoretical model, we found indications of photon-number sensitive Jaynes–Cummings physics in the weak coupling regime of CQED.

4.6 Supplemental material

4.6.1 Detector response

In order to show that the true two-photon correlations are much stronger than the raw experimental data suggests, we present here details on the convolution of the theoretical $g^{(2)}(\tau)$ data with the single-photon counter (SPC) detector response. We use two detectors with 50 ps and 500 ps detector jitter, which was determined by measuring photon correlations of a picosecond Ti:Sapphire laser oscillator. As shown in Fig 4.8 we observe very good agreement between the convoluted theoretical prediction and the experimental data for our QD. Since count rates were high, we could also perform the experiment with a less sensitive 50 ps jitter detector, which again agrees very well to theory. This clearly shows that our $g^{(2)}(\tau)$ measurements are severely reduced by the detector jitter of the single-photon counters, but that we can fully deconvolute this effect.

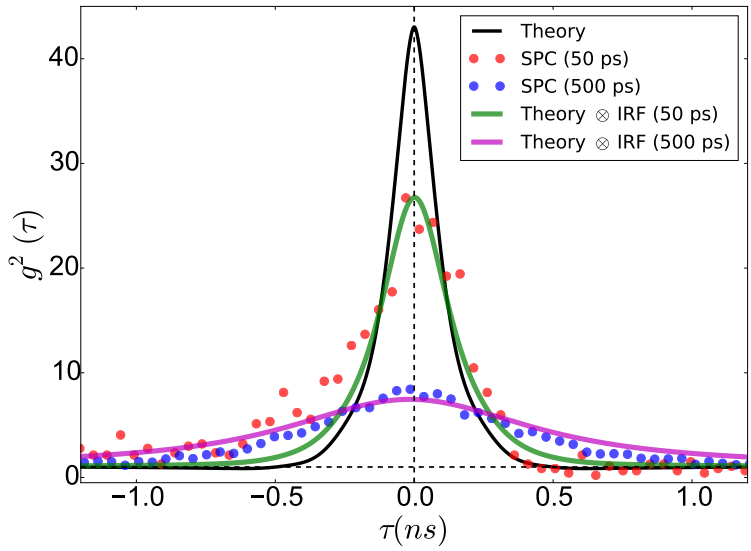

Figure 4.8: Comparison of the theoretical data with and without taking care of detector jitter, and the experimental $g^{(2)}(\tau)$ data for our QD. The agreement between theory and experiment is excellent.

4.6.2 Photon correlations and cavity quality

Here we show that the cavity is essential to obtain the strong photon correlations we observed experimentally. For this we conduct numerical simulations for various cavity decay rates κ. In order to isolate the effect of κ, we have to optimize for each value of κ the laser frequency and the output polarization to find the special polarization angle and thereby the maximum in the $g^{(2)}(0)$ landscape. Next to this we also need to keep the internal mean photon number constant by increasing the incident laser power for a higher value of κ. In order to do this we optimized the power coupling parameter η for each value of κ, so that the mean photon number of the outgoing light (for parallel polarization $\theta_{in} = \theta_{out} = 45°$) on the cavity resonance for an empty cavity remains constant. The result is shown in Fig. 4.9: In the case of almost no cavity (large κ), only very small $g^{(2)}(0)$ values are obtainable, while in good cavities (small κ), extreme values of $g^{(2)}(0)$ are possible. The other parameters for simulation of Fig. 4.9 are similar to those of the device in this chapter.

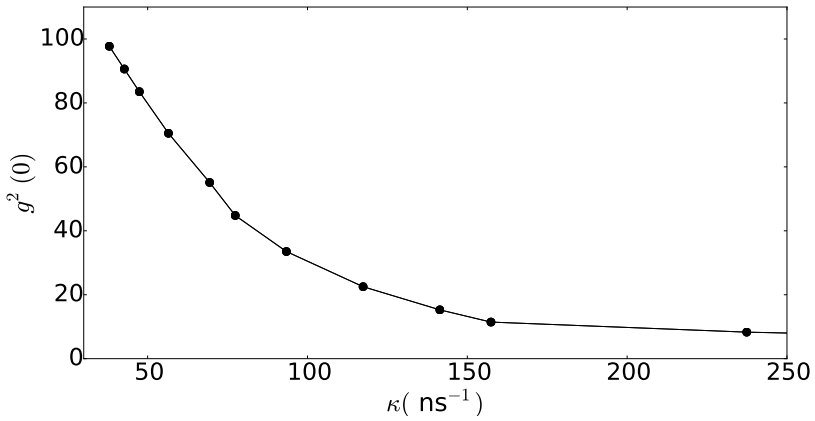

Figure 4.9: Calculated maximal (i.e., for special polarizer angles) $g^{(2)}(0)$ for different cavity decay rates. A good cavity with low κ is needed in order to reach the extreme bunching values $g^{(2)}(0)$.